

Transport Properties of Anisotropic Polar Fluids:

2. Dipolar Interaction

G.A. Fernández, J. Vrabec^{*}, and H. Hasse

Institute of Thermodynamics and Thermal Process Engineering,

University of Stuttgart, D-70550 Stuttgart, Germany

Number of pages: 38

Number of tables: 1

Number of figures: 12

^{*} To whom correspondence should be addressed, tel.: +49-711/685-66107, fax: +49-711/685-66140, email: vrabec@itt.uni-stuttgart.de

ABSTRACT

Equilibrium molecular dynamics simulation and the Green-Kubo formalism were used to calculate self-diffusion coefficient, shear viscosity, and thermal conductivity for 38 different dipolar two-center Lennard-Jones fluids along the bubble line and in the homogeneous liquid. It was systematically investigated how anisotropy, i.e. elongation, and dipole momentum influence the transport properties. The reduced elongation L^* was varied from 0 to 1 and the reduced squared dipole momentum was varied depending on the elongation as follows: for spherical fluids ($L^*=0$) from $\mu^{*2}=0$ to 20, for $L^*=0.2$ from $\mu^{*2}=0$ to 16, and for $L^*=0.4$ and above from $\mu^{*2}=0$ to 12. This represents the entire range in which parameters for real fluids are expected. The statistical uncertainty of the reported data varies with transport property, for self-diffusion coefficient data the error bars are typically lower than 3 %, for shear viscosity and thermal conductivity they are about 8 and 12 %, respectively.

KEYWORDS: Green-Kubo; molecular dynamics; dipole; self-diffusion; shear viscosity; thermal conductivity.

1 INTRODUCTION

In an accompanying work [1] we report on a comprehensive investigation on self-diffusion coefficient, shear viscosity, and thermal conductivity of two-center Lennard-Jones plus point quadrupole (2CLJQ) fluids by equilibrium molecular dynamics and the Green-Kubo formalism. In the present work, that investigation is extended to two-center Lennard-Jones plus point dipole (2CLJD) fluids using the same methodology. These two model types are aimed at molecules with different type of polarity, i.e. 2CLJQ models can well be used for quadrupolar fluids such as CO₂ or Chlorine [2], whereas 2CLJD models are for dipolar fluids such as CO or partly fluorinated alkanes [3].

Static thermodynamic properties of the 2CLJD fluids have been extensively investigated in the past. There are many results for vapor-liquid equilibria [4,5,6,7,8], excess properties [9], or surface tension [10,11]. The 2CLJD potential has been successfully applied to modeling real fluids, yielding good results for vapor-liquid equilibria [12,13,14,3], Joule-Thomson inversion curves [15], virial coefficients [16], and recently also for shear viscosity and thermal conductivity of refrigerants [17]. On the other hand, transport properties for this useful model class have not been explored systematically. An exception is the work of Lee and Cummings [18] on shear viscosity using the Stockmayer potential [19], which is a subgroup ($L^*=0$) of the 2CLJD model fluids investigated here. The present work aims to fill this gap.

This investigation, as the accompanying one on 2CLJQ fluids, is carried out for state points along the bubble line and in the homogeneous liquid. It covers 38 model fluids, specified each by a certain combination of elongation and

dipole momentum. Thermodynamic conditions were selected on the basis of previous work of Stoll et al. [8,20] on vapor-liquid equilibria of 2CLJD fluids. As the present work is analogous to the accompanying one on 2CLJQ fluids [1], redundant information like the Green-Kubo equations is omitted here.

2 MOLECULAR MODEL

The intermolecular interactions are represented by the two-center Lennard-Jones plus point dipole (2CLJD) potential. The 2CLJD potential is pairwise additive and consists out of two identical Lennard-Jones sites a distance L apart (2CLJ) plus a point dipole of momentum μ placed in the geometric center of the molecule, oriented along the molecular axis connecting the two Lennard-Jones (LJ) sites. It is analogous to the quadrupolar 2CLJQ potential investigated in the accompanying work [1], only differing in the polar interaction that is a point dipole instead of a point quadrupole. The contribution of a point dipole is given by [21]

$$u_D = \frac{1}{4\pi\epsilon_0} \frac{\mu^2}{|\mathbf{r}_{ij}^3|} (\sin\theta_i \sin\theta_j \cos\phi_{ij} - 2\cos\theta_i \cos\theta_j), \quad (1)$$

wherein \mathbf{r}_{ij} is the center-center distance vector of two molecules i and j . θ_i is the angle between the axis of the molecule i and the center-center connection line and ϕ_{ij} is the azimuthal angle between the axis of molecules i and j . Finally, ϵ_0 is the electric constant $8.854187817 \cdot 10^{-12} \text{ C}^2/(\text{J m})$.

Analogously to specific 2CLJQ models, a 2CLJD model for a real substance is fully determined by five parameters: σ , ϵ , L , μ [8] and the molecular mass m . In the reduced form also for this model class only two molecular param-

eters remain, i.e. reduced elongation $L^* = L/\sigma$ and reduced squared dipole momentum $\mu^{*2} = \mu^2/(4\pi\epsilon_0\epsilon\sigma^3)$. Henceforth, "squared" will be omitted in the text for brevity.

Furthermore, all results of this study were obtained and are presented in the reduced form; the definitions are given in the accompanying work [1]. For the sake of brevity, "reduced" will be omitted in the following.

3 INVESTIGATED MODELS AND STATES

In the present work, 38 different model fluids were studied, where each fluid is fully determined by one combination of elongation L^* and dipole momentum μ^{*2} . Simulations at 12 liquid state points were carried out for each model fluid.

The studied model fluids have elongations that vary from $L^*=0$, i.e. spherical molecules, to $L^*=1$, i.e. strongly elongated dumbbell-shaped molecules, in seven steps. For Stockmayer fluids, seven dipole momenta from $\mu^{*2}=0$ to 20 were considered. For fluids with $L^*=0.2$, six dipole momenta from $\mu^{*2}=0$ to 16 and for larger elongations five dipole momenta from $\mu^{*2}=0$ to 12 were taken into account. The upper limit of 12 is sufficient to describe strongly dipolar real fluids, e.g. CClF_3 with $\mu = 1.8261$ D ($\mu^{*2} = 3.4932$), CCl_3F with $\mu = 2.7009$ D ($\mu^{*2} = 3.6250$), or $\text{CH}_2\text{F}-\text{CF}_3$ with $\mu = 3.0214$ D ($\mu^{*2} = 8.0004$). Very high dipole momenta ($\mu^{*2}=16$ and 20) were only considered for fluids with a small elongation, because they are realistic only for such molecules [3].

Due to consistency, spherical fluids ($L^*=0$) were treated as two superimposed Lennard-Jones sites. To compare with one-center Lennard-Jones results, the temperature has to be divided by 4 as well as the dipole momentum. Also the

present values of self-diffusion coefficient D^* , shear viscosity η^* , and thermal conductivity λ^* have to be divided by 2.

To facilitate a meaningful comparison of the transport properties, another reduced form of the temperature $T_R=T^*/T_c^*$ and the density $\rho_R=\rho^*/\rho_c^*$ was used, where T_c^* is the critical temperature and ρ_c^* the critical density of the individual 2CLJD fluid; values for T_c^* and ρ_c^* were taken from [8].

For each fluid, three state points along the bubble line were studied from $T_R=0.6$ to 0.9 with temperature increments of $\Delta T_R=0.15$. In addition, another nine state points were studied in the homogeneous liquid on three isochores, starting from these three bubble points with temperature increments of $\Delta T_R=0.15$, cf. Fig. 1. This grid is less dense than the one used in the accompanying work on quadrupolar fluids [1], however, as more model fluids are regarded here, both present roughly the same number of data points.

For quadrupolar fluids critical and bubble densities in terms of ρ^* increase monotonously with increasing quadrupole momentum [8], but dipolar fluids behave different [3]. Fig. 2 illustrates the variation of the bubble density, for three reduced temperatures as a function of the dipole momentum for Stockmayer fluids ($L^*=0$). As can be seen, the critical density, i.e. bubble density at $T_R=1$, increases up to $\mu^{*2} \approx 3$, but decreases for higher dipole momenta. At $T_R=0.9$ and below they are larger than those of non-polar fluids in all cases, where for this temperature a significant maximum of the bubble density at intermediate dipole momenta is present. These tendencies are also found for elongated fluids. The influence of elongation on phase behavior does not differ from that of quadrupolar fluids [1], i.e. bubble densities decrease monotonously with increasing elongation [8].

4 SIMULATION DETAILS

As many of the considerations and technical details of the simulations are the same as those used in the accompanying work [1], we proceed describing only the differences. Here, the significant long range contributions due to the dipolar interaction were treated with the reaction field technique [23,24]. Simulations were carried out in the canonical ensemble using the modified equations of motion with a time step of $\Delta t \sqrt{\epsilon/m}/\sigma = 0.001$, and the Nose-Hoover thermostat [26,27] with a thermal inertial parameter of 10 in reduced units. Statistical uncertainties of the transport coefficients were estimated using the standard deviation of three independent simulations runs with 5 000 independent autocorrelation functions. Independence between correlation functions was achieved with a time span of 0.2 in reduced units between consecutive correlation functions. The convergency issues of self-diffusion coefficient [28] and shear viscosity [29,30,31,32,33] are discussed in the accompanying work [1]. The integrals usually converge within their statistical uncertainties at about 1 in reduced units, nevertheless an integration time of $\Delta t^*=2$ was used.

5 RESULTS

In this section, the simulation results for the transport coefficients are presented. Numerical data for self-diffusion coefficient, shear viscosity, and thermal conductivity are given in Table I for spherical fluids ($L^*=0$) with dipole momenta from $\mu^{*2}=0$ to 20, for slightly elongated fluids ($L^*=0.2$) with dipole momenta from $\mu^{*2}=0$ to 16, and for elongated fluids from $L^*=0.4$ to 1 with dipole momenta ranging from $\mu^{*2}=0$ to 12. All data in Table I correspond to

state points along the bubble line for reduced temperatures of $T_R=0.6$, 0.75, and 0.9. The complete data set, with nine additional state points in the liquid region for each fluid, is available in [34] and partially included in Figs. 5, 6, 8, 9, 11, and 12. The effects of elongation, dipole momentum, temperature, and density are discussed in the following for each transport coefficient separately.

The accuracy of the calculated transport properties decreases in the sequence self-diffusion coefficient, shear viscosity, thermal conductivity. The high accuracy of the self-diffusion coefficient, with error bars lower than 3 %, is due to its individual nature [35]. Shear viscosity and thermal conductivity show larger uncertainties, that are around 8 and 12 %, respectively. In most simulations of the present work the autocorrelation functions of thermal conductivity decay faster than those for shear viscosity, but fluctuate more.

Other factors that influence the accuracy of the reported data are elongation and dipole momentum. In particular, at low temperatures, for fluids with large anisotropy and strong dipole momentum, the transport coefficients show larger simulation uncertainties.

In the following, the results are discussed for ten selected fluids, covering the whole range of the two molecular parameters, from spherical ($L^*=0$) over elongated ($L^*=0.505$) to strongly elongated ($L^*=1.0$) fluids with varying dipole momentum of $\mu^{*2}=0$, 6, 12, and 20. A subset of six fluids is taken in some cases only due to graphical reasons.

5.1 Self-diffusion coefficient

Figs. 3 and 4 illustrate the self-diffusion coefficient along the bubble line for ten selected fluids. The results can either be discussed in terms of reduced density ρ_R as in Fig. 3 or in terms of number density ρ^* as in Fig. 4. From Fig. 3 it can be seen that the regarded range of reduced density is similar for all fluids, but significant deviations from the principle of corresponding states are present also for the density. At constant T_R , it can be discerned that the self-diffusion coefficient always decreases with increasing elongation. The dipole, however, can either decrease or increase the self-diffusion coefficient. A better visibility of the data (which is even more needed for the less accurate properties shear viscosity and thermal conductivity) is obtained when plotted over number density in Fig. 4. Therefore, this graphical representation is preferred in the following.

As Fig. 4 shows, D^* decreases with increasing number density along the bubble line. Self-diffusion coefficients of fully elongated fluids lie roughly along the same line as observed for quadrupolar fluids [1]. To analyze the effect of the dipole momentum, it is helpful to compare the bubble densities of Stockmayer fluids in Fig. 2, where the influence is most visible, with the corresponding self-diffusion coefficients in Fig. 4. The self-diffusion coefficient shows a minimum for Stockmayer fluids with $\mu^{*2} \approx 6$ at all three temperatures. The bubble densities of Stockmayer fluids also show a peculiar behavior: maxima at $T_R=0.9$ and 1 and a point of inflexion at $T_R=0.6$. As the self-diffusion coefficient of non-polar fluids decreases with increasing density, it can be concluded that the isolated effect of the dipole is to increase the self-diffusion coefficient.

Fig. 5 shows the dependence of D^* on number density in the homogeneous liquid region at a constant reduced temperature of $T_R=0.9$. Note that the density range is the same as in Fig. 4. Along this isotherm D^* decreases slightly hyperbolic with increasing density, resembling the behavior of D^* along bubble lines for a given elongation. Comparing D^* along bubble lines with isothermal data for the same density variation, it is found that density is the dominant variable, being responsible for about 80 % of the variation in D^* .

Fig. 6 shows the dependence of the self-diffusion coefficient on reduced temperature for a subset of six selected fluids at different isochores. The isochores correspond to bubble densities at the reduced temperature $T_R=0.6$, cf. Fig. 1, which have similar values in terms of ρ_R . It can be seen that the self-diffusion coefficient decreases monotonously with increasing dipole momentum for elongated fluids, whereas for Stockmayer fluids, D^* again exhibits a minimum at intermediate dipole momenta. Along an isochore, the self-diffusion coefficient increases linearly with increasing temperature. The gradients with respect to reduced temperature are almost constant for a given elongation but less pronounced for more elongated fluids. Such a behavior was also found in the accompanying work on quadrupoles [1].

5.2 *Shear viscosity*

Fig. 7 illustrates the shear viscosity along the bubble line for the ten selected fluids. In contrast to quadrupolar fluids, shear viscosity results for fluids with a given elongation, but different polar momentum, are not along a single line. At constant T_R , shear viscosity increases considerably with increasing dipole momentum. In accordance to quadrupolar fluids [1], more elongated molecules

have generally a lower shear viscosity along the bubble line. The extremely high values of shear viscosity found for high dipole momenta ($\mu^{*2}=20$) at low temperatures are remarkable.

Fig. 8 illustrates the isolated effect of density on shear viscosity for the same ten fluids in the homogeneous liquid region at $T_R=0.9$. Comparing the variation of η^* along bubble lines and along isotherms in the same way as for D^* , it is found that the density effect is responsible for about 80 % of the increase of η^* along the bubble line. Exceptions are the shear viscosities of strongly dipolar Stockmayer fluids with $\mu^{*2}=16$ and 20. These are very sensitive to temperature changes, where the contribution of density is only about 10 % for $\mu^{*2}=20$.

Fig. 9 shows the dependence of shear viscosity on reduced temperature for a subset of six fluids along different isochores with similar values in terms of ρ_R . As expected, the shear viscosity decreases with increasing temperature. Non-polar fluids show little temperature dependence. On the other hand, strongly dipolar fluids, with an about twofold higher shear viscosity than non-polar fluids in the cold liquid, are more sensitive to temperature exhibiting larger gradients.

5.3 Thermal conductivity

Fig. 10 illustrates the thermal conductivity along the bubble line. The thermal conductivity increases with increasing density and more elongated molecules have lower thermal conductivities, similar to quadrupolar fluids [1]. In contrast to quadrupolar fluids, the data for a constant elongation do not lie on a single

line here. It can best be seen for Stockmayer fluids that λ^* increases strongly with increasing dipole momentum at constant T_R .

Fig. 11 shows the density dependence of the same ten fluids in the homogeneous liquid at $T_R=0.9$. As can be seen, the curves resemble those along bubble lines, cf. Fig. 10, demonstrating the dominant density effect. Similar results were found for quadrupolar fluids [1].

Fig. 12 shows the weak temperature dependence of λ^* through isochoric data for a subset of six fluids. Taking the statistical uncertainties and the scatter into account, hardly any trend can be discerned. This is also in agreement to the findings for quadrupolar fluids [1].

6 CONCLUSION

Equilibrium molecular dynamics simulation and the Green-Kubo formalism were used to calculate the self-diffusion coefficient, shear viscosity, and thermal conductivity for 38 different anisotropic and dipolar model fluids. A comprehensive data set was obtained for each fluid and property that covers a substantial part of the liquid state. The statistical uncertainty of the reported data varies according to transport property. For self-diffusion coefficient data it is lower than 3 %, for shear viscosity and thermal conductivity it is around 8 and 12 %, respectively.

It is found that both anisotropy and dipole momentum significantly influence all transport properties along the bubble line. An increasing elongation always leads to lower values, whereas an increasing dipole momentum usually yields higher values. The predominant part of these variations is due to the consid-

erable variations in number density along the bubble line caused by L^* and μ^{*2} . However, peculiar extrema are found, e.g., for the self-diffusion coefficient of fluids with small anisotropy.

Density is the most important thermodynamic variable, however, compared to the findings for quadrupolar fluids [1], it is less dominating and the influence of the dipole is much stronger.

Temperature influences all transport properties less than density. As expected, for higher temperatures the self-diffusion coefficient increases, the shear viscosity decreases, and for the thermal conductivity hardly any variation can be discerned.

List of symbols

D	self-diffusion coefficient
i	molecule index
j	molecule index
L	molecular elongation
m	molecular mass
t	time
T	temperature
u	pair potential
Δ	increment
Δt	integration time step
ϵ	Lennard-Jones energy parameter
ϵ_0	Electric constant
η	shear viscosity

θ angle of nutation
 λ thermal conductivity
 μ molecular dipole momentum
 ρ density
 σ Lennard-Jones size parameter
 ϕ azimuthal angle

Vector properties

\mathbf{r} distance vector

Subscript

c property at critical point
 D point dipole
 R property reduced by critical value

Superscript

$*$ property reduced by molecular parameters

Acknowledgement

We gratefully acknowledge financial support from Deutscher Akademischer Austauschdienst (DAAD).

References

- [1] G.A. Fernández, J. Vrabec, and H. Hasse, Fluid Phase Equilibr., submitted (2006) .
- [2] J. Vrabec, J. Stoll, and H. Hasse, J. Phys. Chem. B **105** (2001) 12126-12133.
- [3] J. Stoll, J. Vrabec, and H. Hasse, J. Chem. Phys. **119** (2003) 11396-11407.
- [4] B. Saager, R. Hennenberg, and J. Fischer, Fluid Phase Equilibr. **71** (1992) 41-66.
- [5] B. Saager, J. Fischer, Fluid Phase Equilibr. **72** (1992) 67-88.
- [6] G.S. Dubey, S.F. Oshea, and P.A. Monson, Mol. Phys. **80** (1993) 997-1007.
- [7] A. Müller, J. Winkelmann, and J. Fischer, J. Chem. Phys. **99** (1993) 3946-3949.
- [8] J. Stoll, J. Vrabec, and H. Hasse, Fluid Phase Equilibr. **209** (2003) 29-53.
- [9] C. Kriebel, A. Müller, J. Winkelmann, and J. Fischer, Mol. Phys. **87** (1996) 151-157.
- [10] M. Mecke, J. Fischer, and J. Winkelmann, J. Chem. Phys. **114** (2001) 5842-5852.
- [11] S. Enders, H. Kahl, M. Mecke, and J. Winkelmann, J. Mol. Liq. **115** (2004) 29-39.
- [12] F. Kohler, N. Van Nhu, Mol. Phys. **80** (1993) 795-800.
- [13] M. Lísal, R. Budinský, V. Vacek, and K. Aim, Int. J. Thermophys. **20** (1999) 163-174.
- [14] C. Kriebel, M. Mecke, J. Winkelmann, J. Vrabec, and J. Fischer, Fluid Phase Equilibr. **87** (1996) 151-157.
- [15] J. Vrabec, G.K. Kedia, and H. Hasse, Cryogenics **45** (2005) 253-258.
- [16] C. Vega, B. Saager, J. Fischer, Mol. Phys. **68** (1989) 1079-1093.
- [17] G.A. Fernández, J. Vrabec, and H. Hasse, Cryogenics, Accepted (2006) .
- [18] S.H. Lee, P.T. Cummings, J. Chem. Phys. **105** (1996) 2044-2055.
- [19] W.H. Stockmayer, J. Chem. Phys. **9** (1941) 392-402.
- [20] J. Stoll, PhD Thesis, Molecular models for the prediction of thermophysical properties of pure fluid and mixtures, Reihe 3, Band 836, VDI, Düsseldorf, 2005.
- [21] C.G. Gray and K.E. Gubbins, Theory of molecular fluids, Vol. 1, Fundamentals, Clarendon Press, Oxford, 1984.
- [22] R. Lustig, Mol. Phys. **65** (1988) 175-179.

- [23] J.A. Barker, R.O. Watts, Mol. Phys. **26** (1973) 789-792.
- [24] M. Neumann, O. Steinhauser, Mol. Phys. **39** (1980) 437-454.
- [25] J.M. Haile, Molecular Dynamics Simulation, John Wiley & Sons, New York, 1997.
- [26] S. Nosé, Mol. Phys. **100** (2002) 191-198.
- [27] D. Frenkel, B. Smit., Understanding molecular simulation, from algorithmus to applications, Academic Press, San Diego California USA, 2002.
- [28] B.J. Alder, in C. Ciccotti and W.G. Hoover (Eds.) , Molecular-dynamic simulation of statistical-mechanical systems, North-Holland, Amsterdam, 1986, pp. 66-76.
- [29] B.J. Alder, D.M. Gass, and T.E. Wainwright, J. Chem. Phys. **53** (1970) 3813-3825.
- [30] G.A. Fernández, J. Vrabec, and H. Hasse, Mol. Sim. **31** (2005) 787-793.
- [31] D. Levesque, L. Verlet, and J. Kürkijarvi, Phys. Rev. A **7** (1973) 1690-1700.
- [32] M. Schoen and C. Hoheisel, Mol. Phys. **56** (1985) 653-672.
- [33] J.J. Erpenbeck, Phys. Rev. A **2** (1974) 2514-2528.
- [34] G.A. Fernández, Transport properties of polar fluids by molecular simulation, PhD Thesis, University of Stuttgart, 2006.
- [35] J.P. Hansen and I.A. McDonald, Theory of Simple Liquids, Academic Press, London, 1986.

Table I

Transport coefficients along bubble lines for 38 2CLJD fluids with different elongations L^* and dipole momentum μ^{*2} . The numbers in parentheses denote the uncertainty in the last digits.

$L^*=0$	T^*	ρ^*	D^*	η^*	λ^*
$\mu^{*2}=0$	3.139	0.8062	0.094(2)	4.65(25)	13.4(6)
	3.925	0.7108	0.202(2)	2.56(16)	9.24(81)
	4.708	0.5838	0.388(8)	1.48(10)	6.29(54)
$\mu^{*2}=3$	3.288	0.8202	0.083(1)	5.46(8)	13.04(89)
	4.110	0.7245	0.184(4)	2.79(39)	10.12(90)
	4.932	0.5966	0.372(7)	1.74(19)	7.26(73)
$\mu^{*2}=6$	3.597	0.8327	0.082(2)	6.02(21)	13.9(10)
	4.494	0.7345	0.183(4)	3.14(35)	10.93(90)
	5.395	0.6049	0.364(7)	1.94(3)	7.36(70)
$\mu^{*2}=9$	3.954	0.8419	0.084(2)	7.44(72)	16.41(31)
	4.943	0.7407	0.187(4)	3.41(19)	13.6(10)
	5.931	0.6082	0.370(7)	1.95(7)	7.01(70)
$\mu^{*2}=12$	4.378	0.8456	0.093(2)	8.99(79)	18.8(12)
	5.470	0.7404	0.199(4)	3.56(20)	14.1(11)
	6.564	0.6024	0.395(8)	1.62(28)	9.32(17)
$\mu^{*2}=16$	4.956	0.8516	0.104(2)	18.8(16)	20.7(21)
	6.192	0.7400	0.215(4)	3.75(23)	15.8(18)
	7.429	0.5968	0.426(9)	1.93(7)	8.91(88)
$\mu^{*2}=20$	5.505	0.8632	0.113(2)	66.4(10)	19.9(12)
	6.878	0.7445	0.226(5)	4.64(1)	14.0(20)
	8.254	0.5972	0.441(9)	2.29(8)	9.93(42)

Table I
Continued.

$L^*=0.2$	T^*	ρ^*	D^*	η^*	λ^*
$\mu^{*2}=0$	2.590	0.7114	0.088(1)	3.64(16)	11.18(62)
	3.237	0.6275	0.190(1)	2.19(7)	8.7(12)
	3.884	0.5144	0.360(8)	1.20(4)	5.66(35)
$\mu^{*2}=3$	2.715	0.7220	0.086(1)	4.21(42)	12.09(95)
	3.393	0.6367	0.189(1)	2.19(6)	10.42(60)
	4.072	0.5244	0.372(2)	1.34(1)	8.30(77)
$\mu^{*2}=6$	2.952	0.7307	0.091(1)	4.27(50)	17.7(11)
	3.691	0.6439	0.197(1)	2.27(18)	15.73(86)
	4.428	0.5306	0.389(1)	1.34(4)	11.3(19)
$\mu^{*2}=9$	3.233	0.7370	0.098(1)	4.22(1)	26.6(16)
	4.040	0.6481	0.211(1)	2.42(5)	22.0(14)
	4.848	0.5315	0.415(2)	1.20(3)	11.9(19)
$\mu^{*2}=12$	3.572	0.7388	0.110(1)	4.32(43)	29.4(21)
	4.464	0.6463	0.235(1)	2.55(34)	24.7(31)
	5.355	0.5226	0.466(1)	1.38(1)	11.5(15)
$\mu^{*2}=16$	3.998	0.7438	0.123(1)	4.75(18)	33.6(55)
	4.997	0.6497	0.258(1)	2.58(23)	25.0(24)
	5.994	0.5229	0.507(2)	1.18(15)	15.9(20)

Table I
Continued.

$L^*=0.4$	T^*	ρ^*	D^*	η^*	λ^*
$\mu^{*2}=0$	1.899	0.5808	0.093(2)	2.51(20)	10.0(22)
	2.374	0.5123	0.187(1)	1.55(7)	7.8(11)
	2.848	0.4185	0.320(3)	0.91(9)	4.84(45)
$\mu^{*2}=3$	1.988	0.5881	0.088(1)	2.97(15)	11.18(60)
	2.485	0.5179	0.182(1)	1.80(18)	9.88(83)
	2.982	0.4262	0.351(2)	0.94(5)	5.90(16)
$\mu^{*2}=6$	2.156	0.5932	0.086(1)	2.86(17)	11.4(12)
	2.695	0.5225	0.182(1)	1.84(6)	9.95(90)
	3.234	0.4275	0.360(1)	0.95(2)	6.22(60)
$\mu^{*2}=9$	2.347	0.5973	0.086(1)	3.52(18)	14.70(57)
	2.934	0.5254	0.186(1)	1.86(5)	10.88(24)
	3.521	0.4296	0.368(1)	0.98(3)	8.02(60)
$\mu^{*2}=12$	2.571	0.5988	0.090(1)	3.49(11)	13.4(15)
	3.214	0.5243	0.194(1)	1.92(19)	12.61(98)
	3.856	0.4257	0.390(1)	1.16(8)	6.88(45)

Table I
Continued.

$L^*=0.505$	T^*	ρ^*	D^*	η^*	λ^*
$\mu^{*2}=0$	1.642	0.5291	0.092(2)	2.24(20)	9.99(84)
	2.052	0.4637	0.184(7)	1.35(10)	6.01(60)
	2.463	0.3835	0.303(8)	0.83(7)	4.16(35)
$\mu^{*2}=3$	1.724	0.5346	0.087(1)	2.66(20)	9.60(79)
	2.155	0.4711	0.175(1)	1.42(13)	8.10(94)
	2.586	0.3854	0.339(1)	0.85(2)	5.33(53)
$\mu^{*2}=6$	1.861	0.5392	0.082(1)	2.92(6)	10.78(16)
	2.327	0.4748	0.171(1)	1.44(2)	7.57(78)
	2.792	0.3902	0.334(2)	0.84(3)	5.09(45)
$\mu^{*2}=9$	2.027	0.5424	0.080(1)	3.11(14)	10.81(69)
	2.535	0.4765	0.171(1)	1.67(11)	9.7(14)
	3.041	0.3898	0.342(1)	0.88(3)	6.47(99)
$\mu^{*2}=12$	2.207	0.5457	0.079(1)	3.38(6)	12.58(20)
	2.759	0.4778	0.175(1)	1.83(3)	10.2(16)
	3.311	0.3886	0.351(2)	0.83(20)	6.92(40)

Table I
Continued.

$L^*=0.6$	T^*	ρ^*	D^*	η^*	λ^*
$\mu^{*2}=0$	1.473	0.4900	0.091(2)	2.16(30)	9.24(46)
	1.842	0.4321	0.174(1)	1.14(1)	6.85(70)
	2.210	0.3520	0.295(9)	0.71(2)	4.15(40)
$\mu^{*2}=3$	1.536	0.4960	0.082(1)	2.19(5)	7.95(31)
	1.920	0.4372	0.166(1)	1.27(7)	5.41(43)
	2.303	0.3597	0.317(1)	0.83(12)	4.78(40)
$\mu^{*2}=6$	1.665	0.4995	0.077(1)	2.08(39)	9.8(18)
	2.082	0.4398	0.160(1)	1.34(7)	7.73(40)
	2.498	0.3583	0.319(1)	0.79(10)	5.12(35)
$\mu^{*2}=9$	1.825	0.5006	0.076(1)	2.91(12)	11.45(41)
	2.281	0.4378	0.165(1)	1.75(15)	7.00(95)
	2.738	0.3545	0.332(1)	0.84(1)	6.22(59)
$\mu^{*2}=12$	1.965	0.5062	0.071(1)	3.28(12)	9.71(44)
	2.456	0.4429	0.159(1)	1.62(4)	7.8(16)
	2.948	0.3603	0.322(1)	0.89(3)	5.94(40)

Table I
Continued.

$L^*=0.8$	T^*	ρ^*	D^*	η^*	λ^*
$\mu^{*2}=0$	1.230	0.4302	0.082(2)	1.79(15)	8.28(42)
	1.538	0.3777	0.157(1)	1.11(14)	4.98(18)
	1.845	0.3051	0.270(5)	0.60(4)	3.86(14)
$\mu^{*2}=3$	1.277	0.4364	0.071(1)	2.18(19)	8.52(31)
	1.596	0.3833	0.145(1)	1.27(14)	6.56(50)
	1.915	0.3101	0.287(1)	0.62(7)	3.67(20)
$\mu^{*2}=6$	1.390	0.4383	0.065(1)	2.25(45)	8.85(65)
	1.738	0.3835	0.141(1)	1.27(8)	5.7(11)
	2.086	0.3085	0.288(1)	0.64(4)	3.39(60)
$\mu^{*2}=9$	1.513	0.4410	0.060(1)	2.44(10)	9.1(10)
	1.891	0.3855	0.137(1)	1.39(1)	7.25(70)
	2.270	0.3093	0.286(2)	0.70(5)	4.32(34)
$\mu^{*2}=12$	1.629	0.4466	0.054(1)	3.02(8)	9.84(80)
	2.036	0.3899	0.130(1)	1.47(2)	7.52(26)
	2.443	0.3155	0.274(1)	0.74(5)	4.92(57)

Table I
Continued.

$L^*=1$	T^*	ρ^*	D^*	η^*	λ^*
$\mu^{*2}=0$	1.058	0.3970	0.0640(5)	1.71(16)	7.12(41)
	1.322	0.3487	0.128(1)	0.98(3)	4.75(35)
	1.587	0.2860	0.245(1)	0.62(6)	3.50(30)
$\mu^{*2}=3$	1.126	0.3976	0.0590(5)	1.96(3)	7.33(39)
	1.408	0.3463	0.127(1)	1.18(6)	4.73(13)
	1.689	0.2793	0.257(1)	0.56(4)	4.09(39)
$\mu^{*2}=6$	1.207	0.4041	0.0480(5)	2.50(9)	7.45(78)
	1.508	0.3524	0.113(1)	1.24(20)	6.04(29)
	1.810	0.2887	0.232(1)	0.67(4)	3.62(17)
$\mu^{*2}=9$	1.308	0.4101	0.0390(5)	3.31(13)	8.54(80)
	1.635	0.3576	0.104(1)	1.56(15)	5.22(18)
	1.961	0.2900	0.228(1)	0.72(5)	4.30(25)
$\mu^{*2}=12$	1.423	0.4163	0.0330(5)	4.09(10)	8.98(30)
	1.779	0.3625	0.0970(5)	1.75(5)	6.64(98)
	2.134	0.2923	0.223(1)	0.75(1)	3.92(34)

List of Figures

- 1 Phase diagrams for two selected elongated 2CLJD fluids ($L^*=0.2$) where one is non-polar and the other strongly dipolar. Saturated densities, taken from [20], are represented by the lines joining at the critical point depicted by \bullet . The investigated state points are indicated by \circ for $\mu^{*2}=0$ and by \triangle for $\mu^{*2}=12$. 27
- 2 Saturated liquid density of Stockmayer fluids ($L^*=0$) for three reduced temperatures ($T_R=0.6, 0.9$, and 1) as functions of the dipole momentum. The solid lines indicate the overall correlation in [8], whereas the symbols are from correlations fitted to each model fluid's vapor-liquid equilibrium individually. 28
- 3 Self-diffusion coefficient of spherical ($L^*=0$, empty symbols), elongated ($L^*=0.505$, grey symbols), and strongly elongated ($L^*=1$, full symbols) 2CLJD fluids over reduced density along bubble lines. Reduced temperatures vary from $T_R=0.6$ to 0.9 . Lines are guides for the eye. 29
- 4 Self-diffusion coefficient of spherical ($L^*=0$, empty symbols), elongated ($L^*=0.505$, grey symbols), and strongly elongated ($L^*=1$, full symbols) 2CLJD fluids over number density along bubble lines. Reduced temperatures vary from $T_R=0.6$ to 0.9 . Lines are guides for the eye. 30

- 5 Self-diffusion coefficient of spherical ($L^*=0$, empty symbols), elongated ($L^*=0.505$, grey symbols), and strongly elongated ($L^*=1$, full symbols) 2CLJD fluids over number density in the homogeneous liquid at $T_R=0.9$. Lines are guides for the eye. 31
- 6 Self-diffusion coefficient of spherical ($L^*=0$, empty symbols) and strongly elongated ($L^*=1$, full symbols) 2CLJD fluids over reduced temperature in the homogeneous liquid along different isochores. \circ : $\rho^*=0.8062$, \triangle : $\rho^*=0.8327$, \diamond : $\rho^*=0.8456$. Lines are guides for the eye. 32
- 7 Shear viscosity of spherical ($L^*=0$, empty symbols), elongated ($L^*=0.505$, grey symbols), and strongly elongated ($L^*=1$, full symbols) 2CLJD fluids over number density along bubble lines. Reduced temperatures vary from $T_R=0.6$ to 0.9 . Lines are guides for the eye. 33
- 8 Shear viscosity of spherical ($L^*=0$, empty symbols), elongated ($L^*=0.505$, grey symbols), and strongly elongated ($L^*=1$, full symbols) 2CLJD fluids over number density in the homogeneous liquid at $T_R=0.9$. Lines are guides for the eye. 34
- 9 Shear viscosity of spherical ($L^*=0$, empty symbols) and strongly elongated ($L^*=1$, full symbols) 2CLJD fluids over reduced temperature in the homogeneous liquid along different isochores. \circ : $\rho^*=0.8062$, \triangle : $\rho^*=0.8327$, \diamond : $\rho^*=0.8456$. Lines are guides for the eye. 35

- 10 Thermal conductivity of spherical ($L^*=0$, empty symbols), elongated ($L^*=0.505$, grey symbols), and strongly elongated ($L^*=1$, full symbols) 2CLJD fluids over number density along bubble lines. Reduced temperatures vary from $T_R=0.6$ to 0.9. Lines are guides for the eye. 36
- 11 Thermal conductivity of spherical ($L^*=0$, empty symbols), elongated ($L^*=0.505$, grey symbols), and strongly elongated ($L^*=1$, full symbols) 2CLJD fluids over number density in the homogeneous liquid at $T_R=0.9$. Lines are guides for the eye. 37
- 12 Thermal conductivity of spherical ($L^*=0$, empty symbols) and strongly elongated ($L^*=1$, full symbols) 2CLJD fluids over reduced temperature in the homogeneous liquid along different isochores. \circ : $\rho^*=0.8062$, \triangle : $\rho^*=0.8327$, \diamond : $\rho^*=0.8456$. Lines are guides for the eye. 38

Fig. 1.

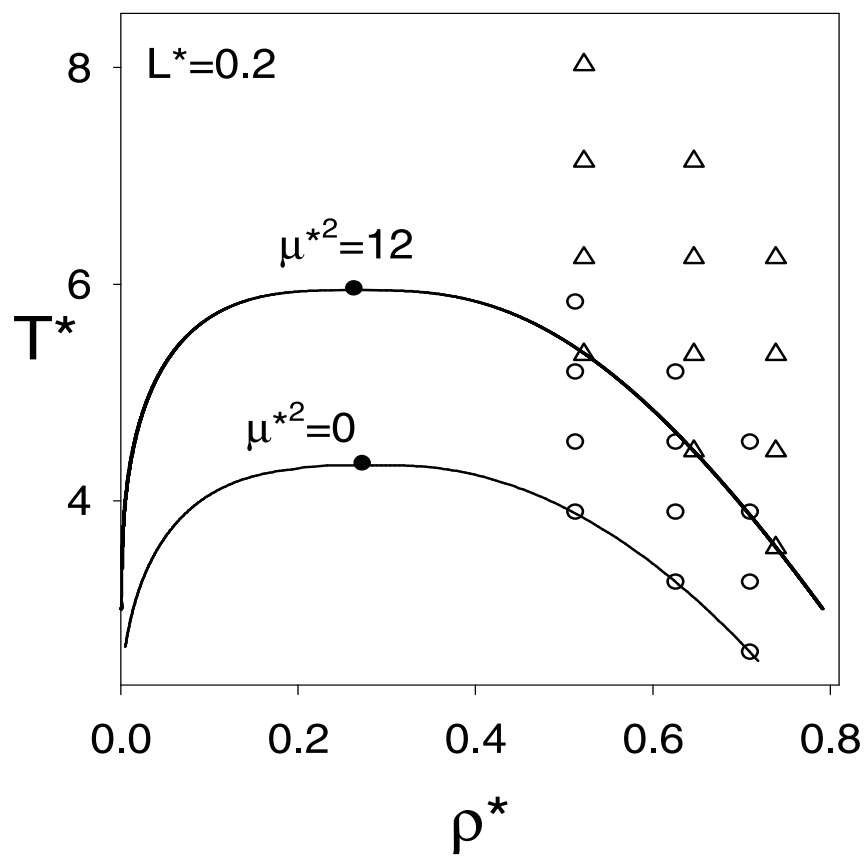


Fig. 2.

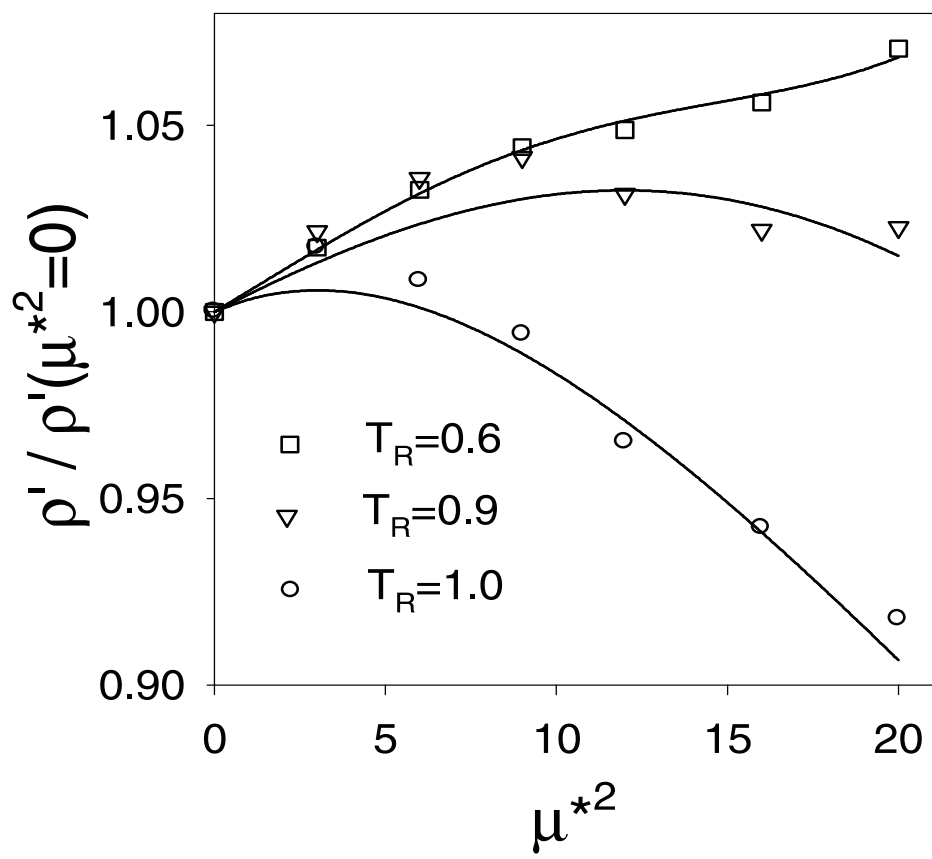


Fig. 3.

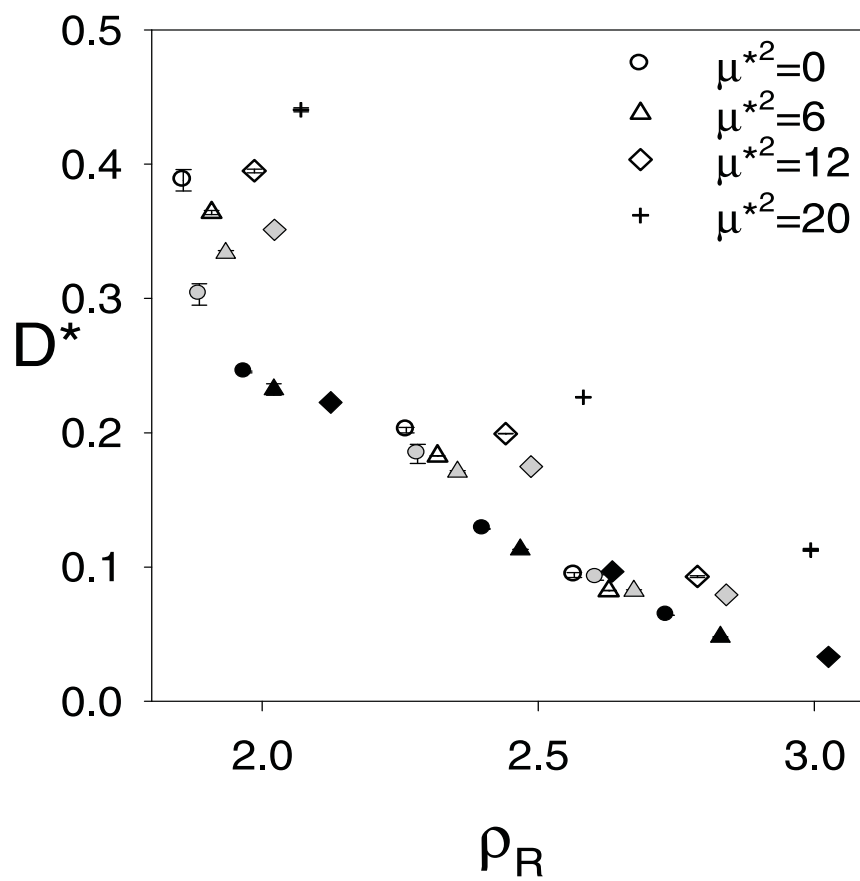


Fig. 4.

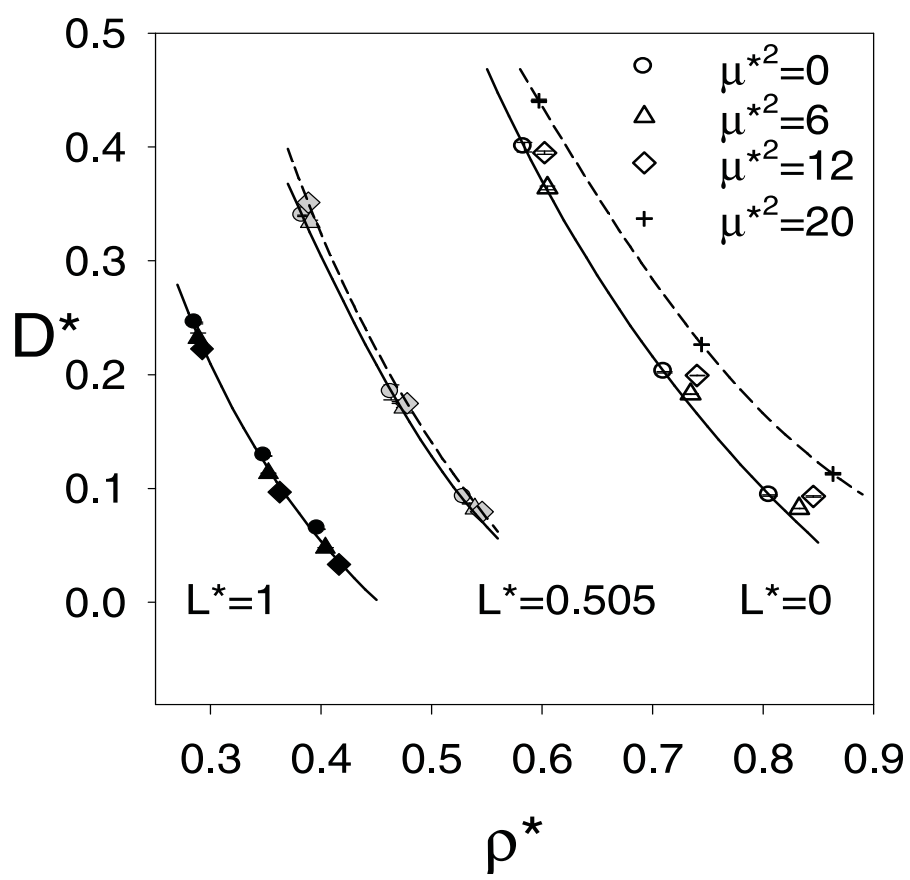


Fig. 5.

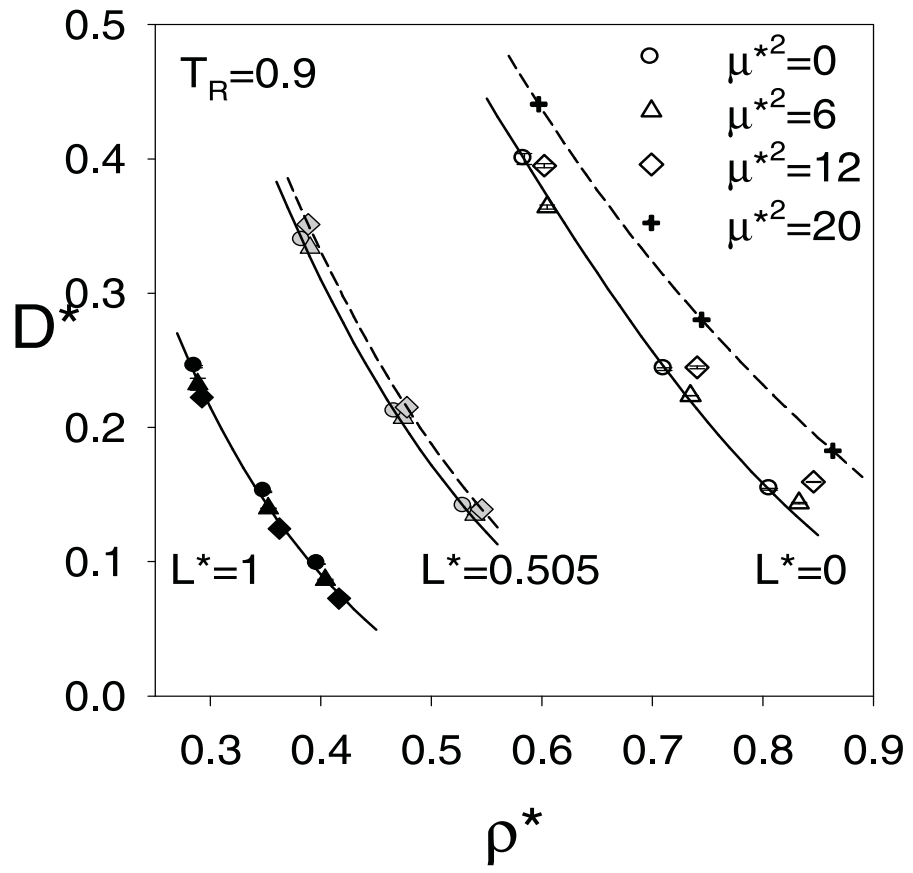


Fig. 6.

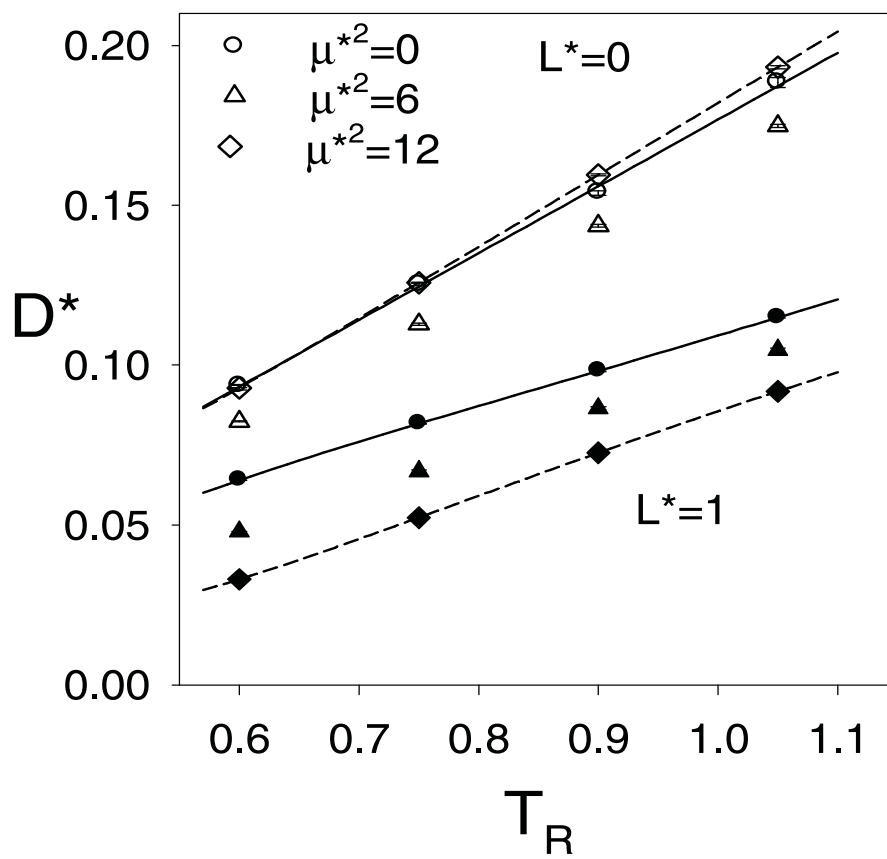


Fig. 7.

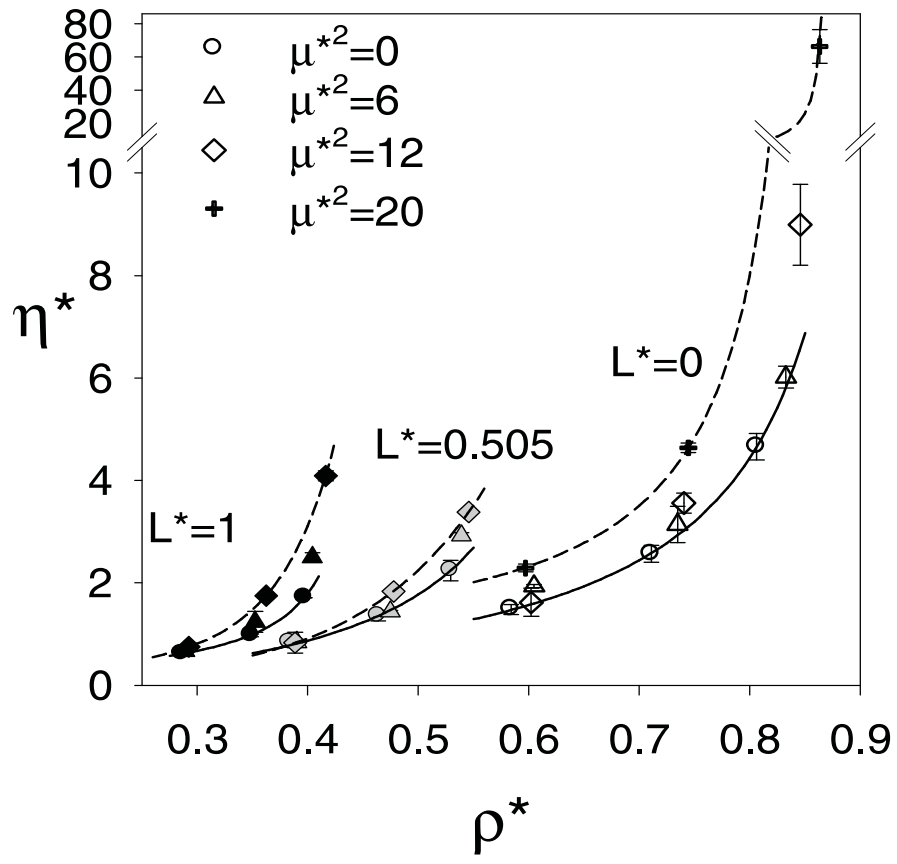


Fig. 8.

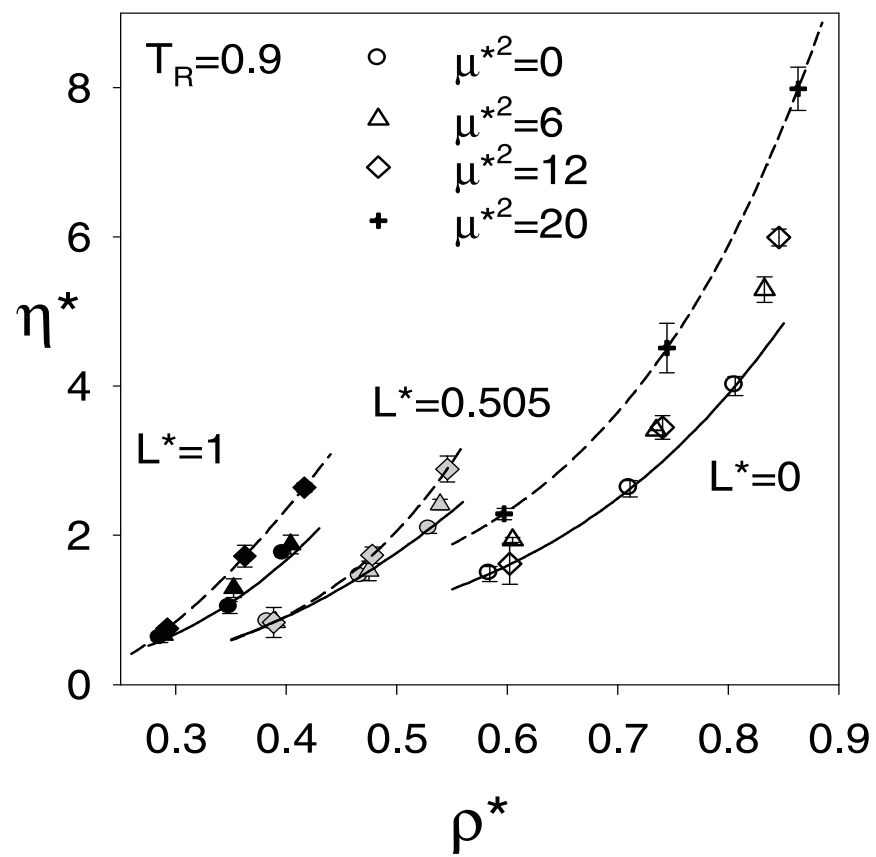


Fig. 9.

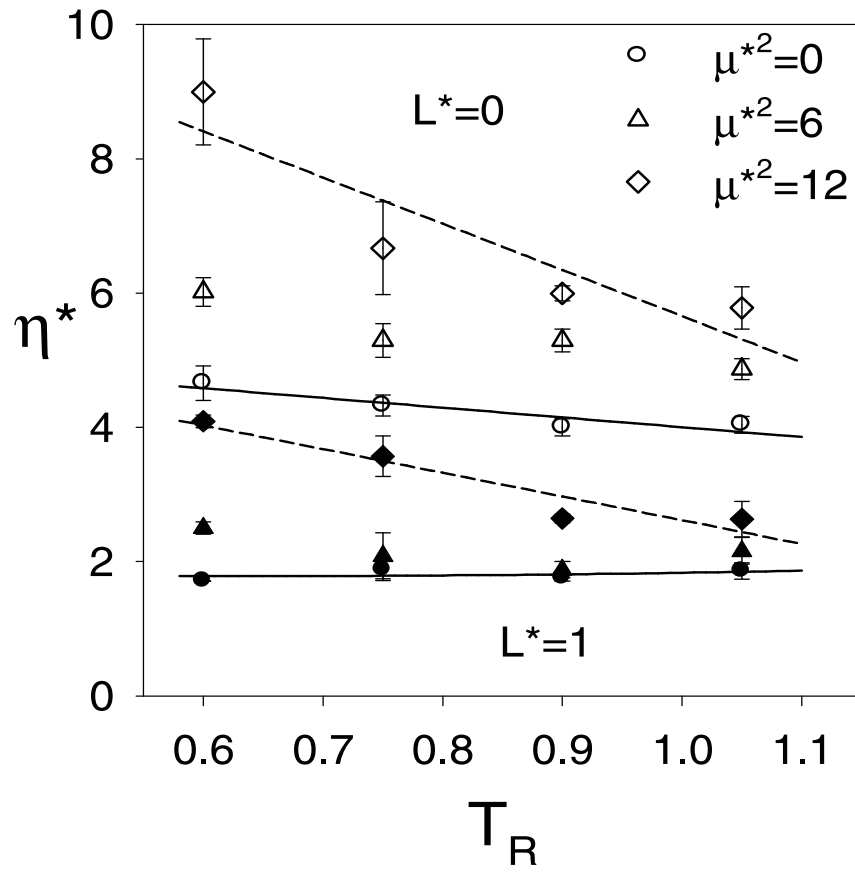


Fig. 10.

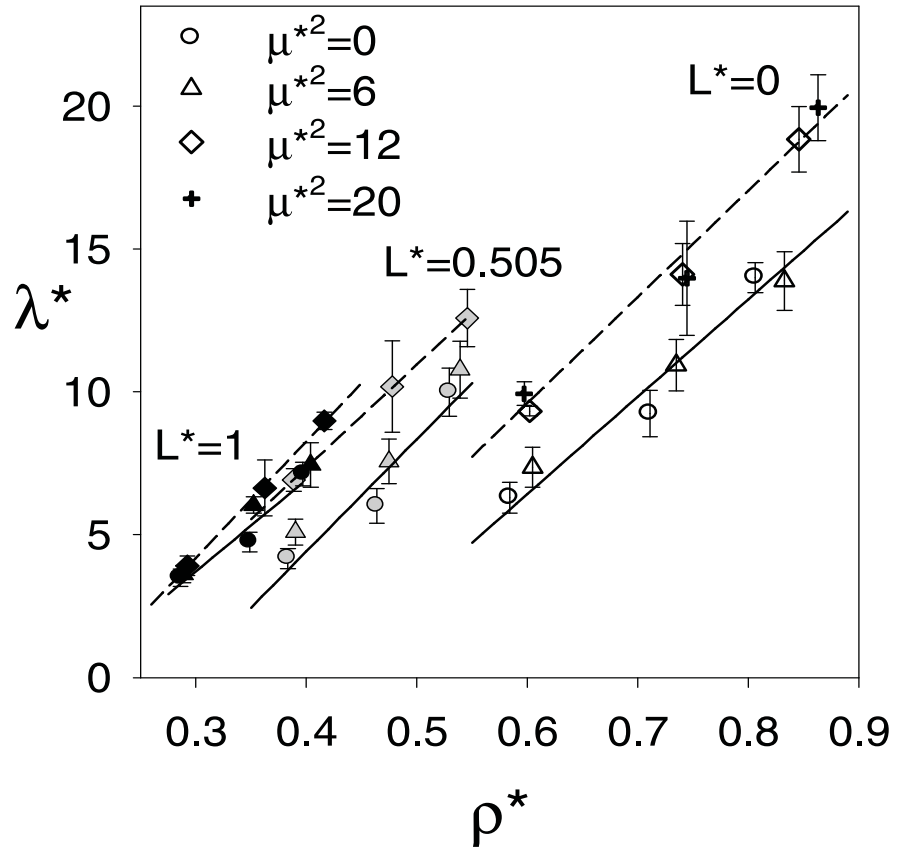


Fig. 11.

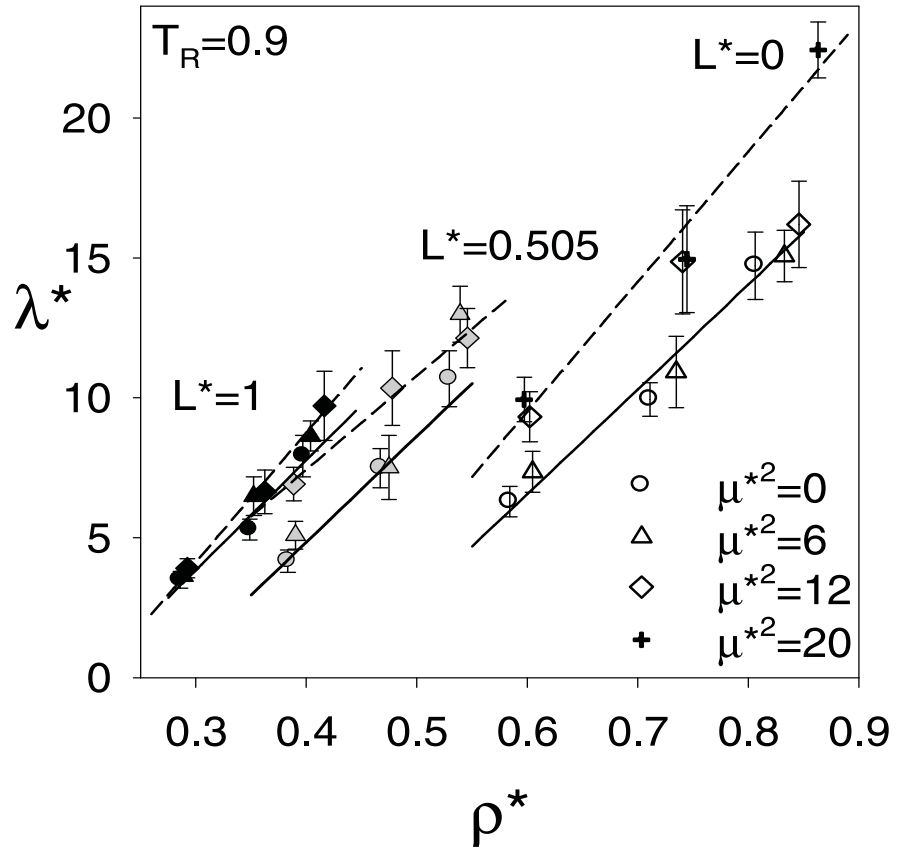


Fig. 12.

